Journal of Power Sources 196 (2011) 10088–10093

Contents lists available at ScienceDirect

Journal of Power Sources

journal homepage: www.elsevier.com/locate/jpowsour

Maximum equivalent power output and performance optimization analysis of an alkaline fuel cell/heat-driven cycle hybrid system

Xiuqin Zhang, Jincan Chen*

Department of Physics, Xiamen University, Xiamen 361005, People's Republic of China

ARTICLE INFO

Article history:
Received 24 June 2011
Received in revised form 2 August 2011
Accepted 2 August 2011
Available online 31 August 2011

Keywords:
Hybrid system
Alkaline fuel cell
Heat-driven cycle
Irreversible loss
Performance analysis
Parametric optimum criterion

ABSTRACT

A generic model of the hybrid system consisting of an alkaline fuel cell (AFC) and a heat-driven cycle, which may work as either a refrigerator or a heat pump, is originally established. On the basis of the models of AFCs and three-heat-reservoir cycles, the equivalent power output and efficiency of the hybrid system are obtained. The performance characteristic curves of the hybrid system are represented through numerical calculation. The maximum equivalent power output and efficiency of the hybrid system are determined. Problems concerning the optimal operation of the hybrid system are discussed. The effects of the main irreversible losses on the performance of the hybrid system are investigated in detail. It is important to note that the waste heat produced in the AFC can be readily used in such a hybrid cycle.

1. Introduction

Alkaline fuel cell (AFC) is one of the most mature fuel cell technologies compared to the others [1,2]. It offers the potential for low cost, good internal thermal management, long lifetime and high efficiency. There is still a need for further improvement in the AFC technology [3–6], such as the cathode and anode development [7–13], the liquid circulating electrolyte analysis [14,15], the application of the anion-exchange poly membrane [16–19], the improvement in the specific conductivity of aqueous potassium hydroxide solutions [20,21], the life cycle assessment [22], and the hybridization of AFC and battery used in electric vehicles [23–25].

AFCs have been in use for more than 30 years by NASA's manned spacecraft, but the cost of the system is still the major barrier if it is to be used in electric vehicles commercially. Since 1970s, the investigations using hydrogen storage alloys as the anode catalyst [26,27] and silver as the cathode catalyst have been developed. At present many cheaper metals such as Ag, Co, or Ni can be used as catalyst [28,29].

When the AFC is used as a power source of electric vehicles or residential areas, the low temperature waste heat produced in the AFC can be utilized to drive a refrigerator or a heat pump rather than a heat engine. Through the combination of an alkaline fuel cell with a heat-driven cycle, not only the performance of the AFC can be enhanced but also an additional refrigerating output or heat-pumping output can be obtained to be used in the vehicle or residential area. Such a hybrid system is similar to an air conditioning absorption refrigeration system in a co-generation process combining a proton exchange membrane fuel cell [30], but is different from solid oxide fuel cell/heat engine hybrid systems [31–35] investigated widely because the high-temperature waste heat produced in the solid oxide fuel cell can be effectively used to drive a heat engine.

In the present paper, the concrete contents are arranged as follows. In Section 2, a generic model of the hybrid system composed of an AFC and a heat-driven cycle is established. The performance of the AFC and the heat-driven cycle is simply described. The equivalent power output and efficiency of the hybrid system are derived. In Section 3, the general performance characteristics of the hybrid system are discussed and the optimum operating regions of some main performance parameters are determined. In Section 4, the effects of the main irreversible losses on the performance of the hybrid system are discussed in detail and some interesting results of the hybrid system under different operating conditions are directly derived. Finally, some important conclusions are summarized.

2. The hybrid system composed of an alkaline fuel cell and a heat-driven cycle

A new hybrid system composed of an AFC and a heat driven cycle is considered, as shown in Fig. 1, where the AFC operated at temperature T acts as the high-temperature heat reservoir of the

* Corresponding author. Tel.: +86 592 2180922; fax: +86 592 2189426.
E-mail address: jcchen@xmu.edu.cn (J. Chen).

0378-7753/$ – see front matter © 2011 Elsevier B.V. All rights reserved.
doi:10.1016/j.jpowsour.2011.08.001

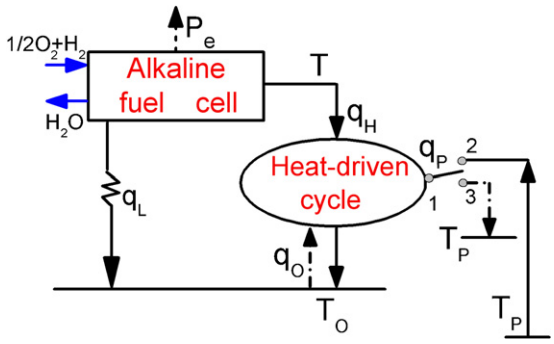

Fig. 1. The schematic diagram of an AFC/heat-driven cycle hybrid system.

heat-driven cycle, q_H is the heat flow from the AFC to the heat-driven cycle, q_P and q_O are, respectively, the heat flows between the heat-driven cycle and the heat reservoirs at temperatures T_P and T_O, q_L is the heat leak directly from the AFC to the environment, and P_e is the electric power output of the AFC. It is very important to note that in the hybrid system, the heat-driven cycle may function as either a refrigerator or a heat pump. When $T_O > T_P$ and switch 1–2 is closed, the heat-driven cycle works as a refrigerator, q_P flows from the cooled space at temperatures T_P to the heat-driven cycle, and q_O flows from the heat-driven cycle to the environment at temperature T_O. When $T_O < T_P$ and switch 1–3 is closed, the heat-driven cycle works as a heat pump, q_P flows from the heat-driven cycle to the heated space at temperatures T_P, and q_O flows from the environment at temperature T_O to the heat-driven cycle. By using such a hybrid system, the waste heat produced in the AFC can be instantly utilized to provide additional cooling or heating and the performance of the system can be improved.

2.1. The power output and efficiency of an alkaline fuel cell

AFC is an electrochemical device that converts the chemical energy of a reaction directly into the electrical and thermal energy. According to Refs. [1,3], the major contributions to irreversible losses in AFC are three overpotential losses including activation overpotential (V_{act}), ohmic overpotential (V_{ohm}), and diffusion overpotential (V_{diff}). The voltage, power output, and efficiency of the AFC can be, respectively, expressed as [3]

$$E = E_{Nernst} - V_{act} - V_{ohm} - V_{diff} = -\frac{\Delta g^0}{n_e F} + \frac{\Delta s^0}{n_e F}(T - 298.15) + \frac{RT}{n_e F}\ln(p_{H_2}\sqrt{p_{O_2}}) - \frac{RT}{\lambda n_e F}\ln\left(\frac{i}{i_0}\right) - i\frac{t_{ele}}{\sigma} + \frac{RT}{\lambda n_e F}\ln\left(1 - \frac{i}{i_L}\right), \quad (1)$$

$$P_e = iA_cE = iA_c\left[-\frac{\Delta g^0}{n_e F} + \frac{\Delta s^0}{n_e F}(T - 298.15) + \frac{RT}{n_e F}\ln(p_{H_2}\sqrt{p_{O_2}}) - \frac{RT}{\lambda n_e F}\ln\left(\frac{i}{i_0}\right) - i\frac{t_{ele}}{\sigma} + \frac{RT}{\lambda n_e F}\ln\left(1 - \frac{i}{i_L}\right)\right], \quad (2)$$

and

$$\eta_e = \frac{P_e}{-\Delta\dot{H}} = \frac{n_e F}{-\Delta h}\left[-\frac{\Delta g^0}{n_e F} + \frac{\Delta s^0}{n_e F}(T - 298.15) + \frac{RT}{n_e F}\ln(p_{H_2}\sqrt{p_{O_2}}) - \frac{RT}{\lambda n_e F}\ln\left(\frac{i}{i_0}\right) - i\frac{t_{ele}}{\sigma} + \frac{RT}{\lambda n_e F}\ln\left(1 - \frac{i}{i_L}\right)\right], \quad (3)$$

where $E_{Nernst} = (-\Delta g^0/(n_e F)) + (\Delta s^0/(n_e F))(T - 298.15) + (RT/(n_e F))\ln(p_{H_2}\sqrt{p_{O_2}})$ is the theoretical maximum potential of the AFC, $V_{act} = (RT/(\lambda n_e F))\ln(i/i_0)$, $V_{ohm} = i(t_{ele}/\sigma)$, $V_{diff} = (-RT/(\lambda n_e F))\ln(1 - i/i_L)$, $-\Delta\dot{H} = (-\Delta h i A_c)/(n_e F)$, Δg^0 and Δs^0 are, respectively, the standard molar Gibbs free energy change and standard molar entropy change at $T = 298.15$ K and $p = 1.00$ atm, n_e is the number of electrons transferred, F is Faraday's constant, R is the universal gas constant, p_{H_2} and p_{O_2} are, respectively, the partial pressures of reactants H_2 and O_2, Δh is the molar enthalpy change at temperature T and $p = 1.00$ atm, λ is the charge transfer coefficient of the electrodes, i is the electric current density, A_c is the surface area of the interconnect plate (assuming that the interconnect plates of AFC have the same area), i_0 is the exchange current density in the electrodes of the AFC, t_{ele} and σ are, respectively, the thickness and specific conductivity of the aqueous electrolyte, and i_L is the limiting current density.

2.2. The coefficient of performance of a heat-driven cycle

The heat-driven cycle in the hybrid system is directly operated among three heat sources and may be referred to as the three-heat-source cycle [36,37]. It has been proved that when the finite-rate heat transfer between the three-heat-source cycle and the heat reservoirs is considered and the cycle of the working substance is assumed to be reversible, the coefficient of performance of the heat-driven cycle for a given rate of heat input q_H may be expressed as [36–38]

$$\psi = \begin{cases} \frac{1}{2}\delta f + \left\{\frac{1}{4}f^2 - \frac{T_P}{T}\left[\frac{(a-1)^2}{a^2} - \frac{T - T_O}{q_H b}\right]\right\}^{\frac{1}{2}} & b > 0 \\ \frac{T_P(T - T_O - q_H b')}{\delta(T_P - T_O)(T - q_H b')} & b = 0 \end{cases}, \quad (4)$$

where $\delta = \begin{cases} 1 & T_p > T_O \\ -1 & T_p < T_O \end{cases}$, $f = \frac{(a-1)^2 T_P - T_O}{Ta^2} - \frac{T_P - T_O}{q_H b} + 1$,

$$a = \left(\frac{1}{\sqrt{U_p}} + \frac{1}{\sqrt{U_O}}\right)\left(\frac{1}{\sqrt{U_p}} + \frac{\delta}{\sqrt{U_H}}\right)^{-1},$$

$$b = \frac{1}{A}\left(\frac{1}{\sqrt{U_p}} + \frac{1}{\sqrt{U_O}}\right)^2, \quad b' = \frac{1}{AU_H},$$

U_H, U_P, and U_O are, respectively, the heat transfer coefficients between the working substance in the cycle and the three heat reservoirs at temperatures T, T_P, and T_O, and A is the total effective heat transfer area of the three-heat-reservoir cycle.

As shown in Fig. 1, one part of the waste heat produced in the AFC is directly released to the environment [39–41] as heat leak q_L, and the other part is transferred to the three-heat-source cycle in the hybrid system. The heat leak may be expressed as [42,43]

$$q_L = K_l A_l (T - T_O), \quad (5)$$

where K_l is the convective and/or conductive heat leak coefficient and A_l is the effective heat transfer area. According to the first law of thermodynamics and Fig. 1, one can derive the rate of heat input from the AFC to the three-heat-source cycle as

$$q_H = -\Delta\dot{H} - P_e - q_L. \quad (6)$$

Substituting Eqs. (3) and (5) into Eq. (6) yields

$$q_H = \frac{-A_c\ \Delta h}{n_e F}[(1 - \eta_e)i - b_1(T - T_O)], \quad (7)$$

Table 1
Parameters used in the model of an AFC.

Parameter	Value
Number of electrons, n_e	2
Faraday constant, F (C mol^{-1})	96,485
Standard molar entropy change, Δs^0 (J mol^{-1})	−163.4
Standard molar Gibbs free energy change, Δg^0 (kJ mol^{-1})	−237.3
Universal gas constant, R (J mol^{-1} K^{-1})	8.314
Charge transfer coefficient of the electrodes, λ	0.1668
Thickness of the electrolyte, t_{ele} (m)	0.001
Limiting current density, i_L (A m^{-2})	5000

where $b_1 = K_l A_l n_e F/(-A_c\,\Delta h)$. Substituting Eq. (7) into Eq. (4), one can obtain the coefficient of performance ψ and rate of heat flow q_P of the three-heat-source cycle as

$$\psi = \begin{cases} \frac{1}{2}\delta f + \left\{\frac{1}{4}f^2 - \frac{T_P}{T}\left[\frac{(a-1)^2}{a^2} - \frac{1}{b_2}\frac{T-T_O}{(1-\eta_e)i - b_1(T-T_O)}\right]\right\}^{1/2} \\ \quad b_2 > 0 \\ \frac{T_P\{T-T_O-b_2'[(1-\eta_e)i - b_1(T-T_O)]\}}{\delta(T_P-T_O)\{T-b'_2[(1-\eta_e)i - b_1(T-T_O)]\}} \\ \quad b_2 = 0 \end{cases} \tag{8}$$

and

$$q_P = q_H\psi = \frac{-A_c\,\Delta h}{n_e F}[(1-\eta_e)i - b_1(T-T_O)]\psi, \tag{9}$$

where $f = ((a-1)^2T_P - T_O)/(Ta^2) - (T_P - T_O)/(b_2[(1-\eta_e)i - b_1(T-T_O)]) + 1$, $b_2 = ((-A_c\,\Delta h)/(An_eF))(1/\sqrt{U_P} + 1/\sqrt{U_O})^2$, and $b_2' = (-A_c\,\Delta h)/(An_eFU_H)$.

2.3. The equivalent power output and efficiency of the hybrid system

Using Eqs. (3) and (7)–(9), we can derive the equivalent power output and efficiency of the hybrid system as

$$P = P_e + q_P\left(1 - \frac{T_O}{T_P}\right)\delta = \frac{-A_c\,\Delta h}{n_e F}\left\{i\eta_e + \delta\psi\left(1 - \frac{T_O}{T_P}\right) \times [(1-\eta_e)i - b_1(T-T_O)]\right\} \tag{10}$$

and

$$\eta = \frac{P_e + q_P(1-(T_O/T_P))\delta}{-\Delta\dot{H}} = \eta_e + \delta\psi\left(1 - \frac{T_O}{T_P}\right)\left[1 - \eta_e - \frac{b_1}{i}(T-T_O)\right]. \tag{11}$$

It should be pointed out that although the model established here is an idealized one, it can be conveniently used to evaluate the performance characteristics of the hybrid system and discuss the optimum design and operation of real fuel cell/heat-driven cycle hybrid systems.

3. General performance characteristics and parametric optimum criteria

It is found from Eqs. (1)–(3) and (8)–(11) that the performance of the hybrid system lies on a series of electrochemical and thermodynamic parameters such as the working current density i of the AFC, temperatures T, T_P, and T_O, and the synthesis parameters a, b_1, b_2, and b_2' of the hybrid system. On the basis of the parameters summarized in Tables 1 and 2 which are obtained from the data available in literature [1,3,9,20], the following numerical calculations are carried out.

Table 2
The values of some parameters at temperature 353 K.

T (K)	Δh (kJ mol^{-1})	p_{H_2} (atm)	p_{O_2} (atm)	σ (S m^{-1})	i_0 (A m^{-2})
353	−284.3	2.530	0.4459	123.5	0.0314

Equation (1) can be used to generate the curve of the output voltage E varying with the current density i of the AFC, as shown in Fig. 2. It is seen from Fig. 2 that E of the AFC is a monotonically decreasing function of i. When $i = i_{max}$, E is equal to zero. Thus, the current density i of the AFC is always smaller than i_{max}.

Using Eqs. (2), (3) and (8)–(11), one can plot the curves of the equivalent power density $P^* = PA_c^{-1}$ and the equivalent efficiency η of the hybrid system varying with the current density i, as shown in Figs. 3 and 4, respectively. Figs. 3 and 4 clearly show that the performance of the hybrid system is much better than that of a single AFC or three-heat-source cycle. For example, based on the parameters adopted here, the maximum equivalent power output of the hybrid system including a refrigerator is 1.4 times of that of a single AFC or 3.3 times of that of a single refrigerator. Meanwhile the maximum equivalent power output of the hybrid system including a heat pump is 2.4 times of that of a single AFC or 1.2 times of that of a single heat pump. It is seen from Figs. 3 and 4 that there exist a maximum equivalent power density P^*_{max} and a maximum equivalent efficiency η_{max} for the hybrid system, with

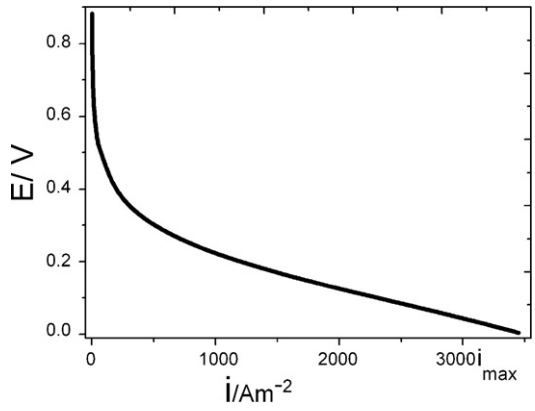

Fig. 2. The output voltage versus current density curve of the AFC, where i_{max} is the maximum current density.

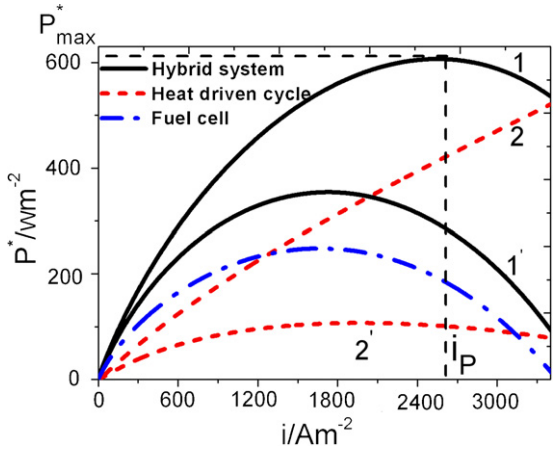

Fig. 3. The equivalent power output density versus current density curves of the hybrid system for $T = 353$ K, $U_H = U_P = U_O$, $b_1 = b_2 = 0.01$, where i_P is the current density at the maximum equivalent power output density P^*_{max}. Curves 1 and 2 correspond to the case of $T_P = 300$ K and $T_O = 273$ K and Curves 1′ and 2′ correspond to the case of $T_O = 300$ K and $T_P = 273$ K.

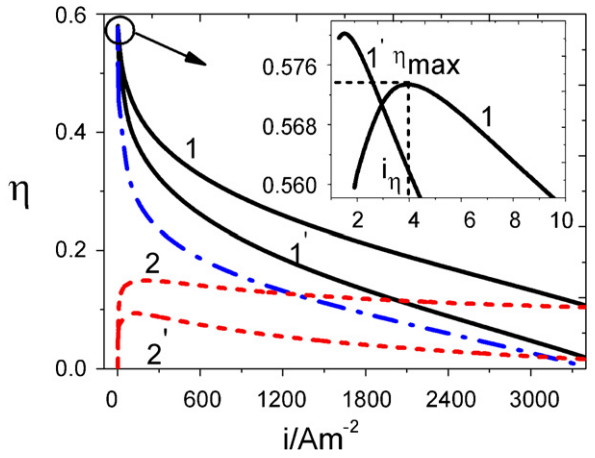

Fig. 4. The equivalent efficiency versus current density curves of the hybrid system, where i_η is the current density at the maximum equivalent efficiency η_{max}. The values of the other parameters are the same as those used in Fig. 3.

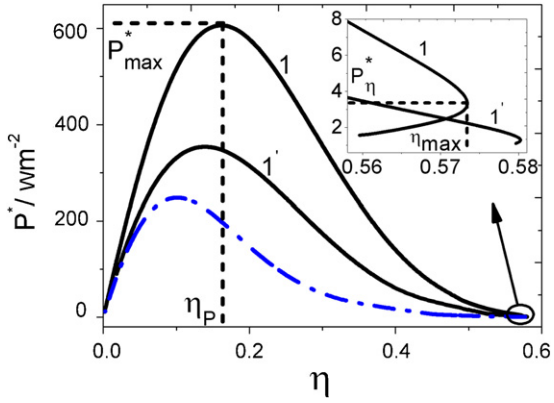

Fig. 5. The equivalent power output density versus equivalent efficiency curves, where η_P is the equivalent efficiency at the maximum equivalent power output density P^*_{max} and P^*_η is the equivalent power output density at the maximum equivalent efficiency η_{max}. The values of the other parameters are the same as those used in Fig. 3.

the corresponding current densities i_P and i_η, respectively. It is also seen from Figs. 3 and 4 that in the region of $i < i_\eta$, the equivalent power density and efficiency of the hybrid system will decrease as the current density i is decreased, while in the region of $i > i_P$, the equivalent power density and efficiency of the hybrid system will decrease as the current density i is increased. It shows clearly that although the regions of $0 \le i < i_\eta$ and $i_{max} \ge i > i_P$ are the possibly working regions of the hybrid system, they are not optimal regions. Obviously, the optimal working region of the current density should be situated between i_η and i_P, i.e.,

$$i_\eta \le i \le i_P. \tag{12}$$

It shows that i_P and i_η are two important parameters of the hybrid system as they determine the upper and lower bounds of the optimized current density, respectively.

When the current density is operated in the optimal region determined by Eq. (12), the equivalent power density of the hybrid system will increase as the equivalent efficiency is decreased, and vice versa, as shown in Fig. 5, where η_P is the equivalent efficiency at the maximum equivalent power density and P^*_η is the equivalent power density at the maximum equivalent efficiency. It is clearly seen from Fig. 5 that η_{max} and P^*_{max} give the upper bounds of the equivalent efficiency and power density, while η_P and P^*_η determine the lower bounds of the optimized values of the equivalent efficiency and power density. Thus, the optimal operating regions of the equivalent power density and efficiency of the hybrid system should be, respectively, determined by

$$P^*_{max} \ge P \ge P^*_\eta \tag{13}$$

and

$$\eta_P \le \eta \le \eta_{max}. \tag{14}$$

It is also seen from Fig. 5 that for an AFC hybrid system, the equivalent power density P^*_η at the maximum efficiency η_{max} is very small and almost equal to zero. It can be proved that the product of P^*_{max} and η_P is much larger than that of P^*_η and η_{max}. Therefore, the AFC hybrid system should, in general, be operated around the state of the maximum equivalent power output, unless there are special requirements for the efficiency.

4. Discussion

It is very important to note that the model established here can be used to explore the effects of some key parameters on the performance of the hybrid system. Below, the effects of synthesis parameters b_1, b_2, and b'_2 will be discussed in detail.

4.1. Influence of b_1

When the heat leak in the AFC is negligible, $b_1 = 0$. In such a case, Eqs. (10) and (11) may be, respectively, simplified as

$$P = \frac{-iA_c\ \Delta h}{n_e F}\left[\eta_e + \psi\delta\left(1 - \frac{T_O}{T_P}\right)(1-\eta_e)\right] \tag{15}$$

and

$$\eta = \eta_e + \psi\delta\left(1 - \frac{T_O}{T_P}\right)(1-\eta_e), \tag{16}$$

where

$$\psi = \begin{cases} \frac{1}{2}\delta f + \left\{\frac{1}{4}f^2 - \frac{T_P}{T}\left[\frac{(a-1)^2}{a^2} - \frac{T-T_O}{b_2(1-\eta_e)i}\right]\right\}^{1/2} & b_2 > 0 \\ \frac{T_P[T - T_O - b'_2(1-\eta_e)i]}{\delta(T_P - T_O)[T - b'_2(1-\eta_e)i]} & b_2 = 0 \end{cases}$$

and

$$f = \frac{(a-1)^2 T_P - T_O}{Ta^2} - \frac{T_P - T_O}{b_2(1-\eta_e)i} + 1.$$

Combining Eqs. (3), (15) and (16), one can generate the performance characteristic curves of the AFC/heat-driven cycle hybrid system, as shown by curves 1, 3, and 5 in Figs. 6 and 7, respectively. If $b_1 > 0$, the performance characteristic curves of the AFC/heat-driven cycle hybrid system are, respectively, shown by curves 1 and 1′ in Figs. 3–5. It can be proved from Eqs. (10) and (11) that the equivalent power output and efficiency of the hybrid system are monotonically decreasing functions of b_1.

4.2. Influence of b_2

When $U_P \to \infty$ and $U_O \to \infty$, $b_2 = 0$. In such a case, combining Eqs. (8), (10) and (11), one can derive the equivalent power output and efficiency of the hybrid system as

$$P = \frac{-iA_c\ \Delta h}{n_e F}\left[\eta_e + \frac{T - T_O - b'_2[(1-\eta_e)i - b_1(T-T_O)]}{T - b'_2[(1-\eta_e)i - b_1(T-T_O)]} \times \left[1 - \eta_e - \frac{b_1}{i}(T - T_O)\right]\right] \tag{17}$$

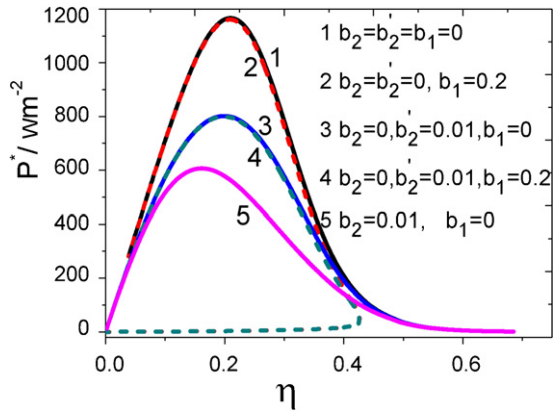

Fig. 6. The equivalent power output density versus equivalent efficiency curves of the AFC/heat pump hybrid system for $T = 353$ K, $T_P = 300$ K, and $T_O = 273$ K.

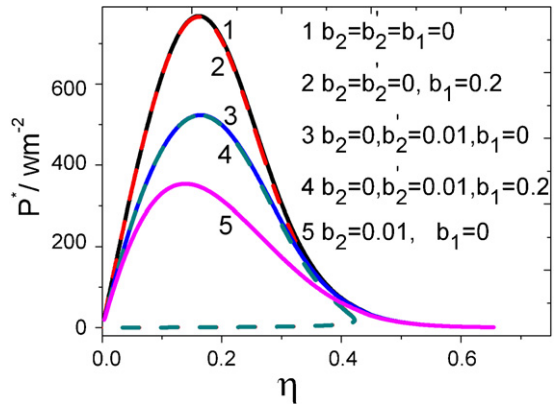

Fig. 7. The equivalent power output density versus equivalent efficiency curves of the AFC/refrigerator hybrid system for $T = 353$ K, $T_O = 300$ K, and $T_P = 273$ K.

and

$$\eta = \eta_e + \frac{T - T_O - b'_2[(1-\eta_e)i - b_1(T-T_O)]}{T - b'_2[(1-\eta_e)i - b_1(T-T_O)]} \times \left[1 - \eta_e - \frac{b_1}{i}(T - T_O)\right], \quad (18)$$

respectively. The performance characteristic curves of the AFC/heat-driven cycle hybrid system are shown by curves 1–4 in Figs. 6 and 7. When $b_1 = 0$, Eqs. (17) and (18) may be further simplified as

$$P = \frac{-iA_c\ \Delta h}{n_e F}\left\{\eta_e + (1-\eta_e)\left[1 - \frac{T_O}{T - b'_2(1-\eta_e)i}\right]\right\} \quad (19)$$

and

$$\eta = \eta_e + \frac{(1-\eta_e)[T - T_O - b'_2(1-\eta_e)i]}{T - b'_2(1-\eta_e)i}, \quad (20)$$

respectively. The performance characteristic curves of the hybrid system are shown by curves 1, 3 in Figs. 6 and 7.

4.3. Influence of b'_2

When $U_H \to \infty$, $U_P \to \infty$, and $U_O \to \infty$, $b_2 = b'_2 = 0$. Eqs. (17) and (18) can be, respectively, simplified as

$$P = \frac{-iA_c\ \Delta h}{n_e F}\left\{\eta_e + \frac{T - T_O}{T}\left[1 - \eta_e - \frac{b_1}{i}(T - T_O)\right]\right\} \quad (21)$$

and

$$\eta = \eta_e + \frac{T - T_O}{T}\left[1 - \eta_e - \frac{b_1}{i}(T - T_O)\right]. \quad (22)$$

The performance characteristic curves of the hybrid system are shown by curves 1 and 2 in Figs. 6 and 7. When $b_1 = 0$, Eqs. (21) and (22) may be further simplified as

$$P = \frac{-iA_c\ \Delta h}{n_e F}\left[1 + \frac{T_O}{T}(\eta_e - 1)\right] \quad (23)$$

and

$$\eta = 1 + \frac{T_O}{T}(\eta_e - 1). \quad (24)$$

The performance characteristic curves of the hybrid system are shown by curves 1 in Figs. 6 and 7.

When $b_2 > 0$ and $b'_2 > 0$, it can be proved from Eqs. (8), (10) and (11) that the equivalent power output and efficiency of the hybrid system are monotonically decreasing functions of b_2 and b'_2.

4.4. Two interesting cases of the hybrid system

Using Eqs. (3), (10), (11) and (15)–(24), one can discuss the performance characteristics of the hybrid system operated under the different conditions of $T_O < T_P$ and $T_O > T_P$.

When $T_O < T_P$ and switch 1–3 in Fig. 1 is closed, the hybrid system is composed of an AFC and a three-heat-source heat pump. Using Eqs. (3), (10), (11) and (15)–(24), one can obtain the performance characteristic curves of the AFC/heat pump hybrid system operated at different conditions, as shown by the curves in Fig. 6 and curve 1 in Figs. 3–5.

When $T_O > T_P$ and switch 1–2 in Fig. 1 is closed, the hybrid system is composed of an AFC and a three-heat-source refrigerator. Using Eqs. (3), (10), (11) and (15)–(24), one can obtain the performance characteristic curves of the hybrid system operated at different conditions, as shown by the curves in Fig. 7 and curve 1′ in Figs. 3–5.

As mentioned previously, the heat-driven cycle in the hybrid system may work as either a refrigerator or a heat pump through the switch control in Fig. 1. Thus, the hybrid system may play different functions according to different practical needs to fully utilize the waste heat produced in the AFC.

5. Conclusions

A combined cycle model composed of an AFC and a heat-driven cycle has been originally established by using the previously developed models of AFCs and three-heat-source cycles. The irreversible losses of the hybrid system resulting from the electrochemical reaction in the AFC and finite-rate heat transfer in the three-heat-source cycle are synthetically considered. Expressions for the equivalent power output and efficiency of the hybrid system are derived and used to discuss its optimal performance. It is shown that such a hybrid system can effectively reuse the low temperature waste heat produced in the AFC to increase the maximum equivalent power output of the system. The optimal operating regions of some important parameters including the equivalent power output, equivalent efficiency, and current density of the hybrid system are determined. The results obtained here may provide some theoretical guidance for the optimal design and operation of practical AFC/heat-driven cycle hybrid systems.

Acknowledgments

The authors would like to thank Dr. Yingru Zhao (Department of Chemical Engineering, Imperial College, London, UK) for useful discussions. This work has been supported by the National

Natural Science Foundation (No. 51076134) and the Fundamental Research Fund for the Central Universities (No. 201112G007), People's Republic of China.

References

[1] B.Y.S. Lin, D.W. Kirk, S.J. Thorpe, J. Power Sources 161 (2006) 474–483.
[2] E. Gülzow, J. Power Sources 61 (1996) 99–104.
[3] I. Verhaert, M. De Paepe, G. Mulder, J. Power Sources 193 (2009) 233–240.
[4] K. Tomantschger, F. Mcclusky, L. Oporto, A. Reid, J. Power Sources 18 (1986) 317–335.
[5] T. Burchardt, P. Gouérec, E. Sanchez-Cortezon, Z. Karichev, J.H. Miners, Fuel 81 (2002) 2151–2155.
[6] A. Tewari, V. Sambhy, M.U. Macdonald, A. Sen, J. Power Sources 153 (2006) 1–10.
[7] F. Bidault, D.J.L. Brett, P.H. Middleton, N. Abson, N.P. Brandon, Int. J. Hydrogen Energy 35 (2010) 1783–1788.
[8] F. Bidault, D.J.L. Brett, P.H. Middleton, N.P. Brandon, J. Power Sources 187 (2009) 39–48.
[9] E. Han, İ. Eroğlu, L. Türker, Int. J. Hydrogen Energy 25 (2000) 157–165.
[10] E. Gülzow, M. Schulze, G. Steinhilber, J. Power Sources 106 (2002) 126–135.
[11] C. Coutanceau, L. Demarconnay, C. Lamy, J.-M. Léger, J. Power Sources 156 (2006) 14–19.
[12] N.A. Popovich, R. Govind, J. Power Sources 112 (2002) 36–40.
[13] J.H. Kim, S. Yonezawa, M. Takashima, Int. J. Hydrogen Energy 35 (2010) 8707–8714.
[14] M. Cifrain, K.V. Kordesch, Advances, J. Power Sources 127 (2004) 234–242.
[15] P. Gouérec, L. Poletto, J. Denizot, E. Sanchez-Cortezon, J.H. Miners, J. Power Sources 129 (2004) 193–204.
[16] C. Sollogoub, A. Guinault, C. Bonnebat, M. Bennjima, L. Akrour, J.F. Fauvarque, L. Ogier, J. Membr. Sci. 335 (2009) 37–42.
[17] M. Guo, J. Fang, H. Xu, W. Li, X. Lu, C. Lan, K. Li, J. Membr. Sci. 362 (2010) 97–104.
[18] Y. Wu, C. Wu, T. Xu, X. Lin, Y. Fu, J. Membr. Sci. 338 (2009) 51–60.
[19] Y. Wan, B. Peppley, K.A.M. Creber, V.T. Bui, E. Halliop, J. Power Sources 185 (2008) 183–187.
[20] R.J. Gilliam, J.W. Graydon, D.W. Kirk, S.J. Thorpe, Int. J. Hydrogen Energy 32 (2007) 359–364.
[21] A. Verma, S. Basu, J. Power Sources 145 (2005) 282–285.
[22] I. Staffell, A. Ingram, Int. J. Hydrogen Energy 35 (2010) 2491–2505.
[23] E.D. Geeter, M. Mangan, S. Spaepen, W. Stinissen, G. Vennekens, J. Power Sources 80 (1999) 207–212.
[24] K. Kordesch, J. Gsellmann, M. Cifrain, S. Voss, V. Hacker, R.R. Aronson, et al., J. Power Sources 80 (1999) 190–197.
[25] M. Duerr, S. Gair, A. Cruden, J. McDonald, J. Power Sources 171 (2007) 1023–1032.
[26] Y. Chen, C. Sequeira, T. Allen, C.P. Chen, J. Alloy Compd. 404–406 (2005) 661–664.
[27] W.K. Hu, D. Noréus, J. Alloy Compd. 356–357 (2003) 734–737.
[28] J.R. Varcoe, R.C.T. Slade, Fuel Cells 5 (2005) 187–200.
[29] H. Jung, K. Fujii, T. Tamaki, H. Ohashi, T. Ito, T. Yamaguchi, J. Membr. Sci. 373 (2011) 107–111.
[30] I. Pilatowsky, R.J. Romero, C.A. Isaza, S.A. Gamboa, W. Rivera, P.J. Sebastian, J. Moreira, Int. J. Hydrogen Energy 32 (2007) 3174–3182.
[31] P. Costamagna, L. Magistri, A.F. Massardo, J. Power Sources 96 (2001) 352–368.
[32] S.H. Chan, H.K. Ho, Y. Tian, J. Power Sources 109 (2002) 111–120.
[33] F. Calise, A. Palombo, L. Vanoli, J. Power Sources 158 (2006) 225–244.
[34] M. Granovskii, I. Dincer, M.A. Rosen, J. Power Sources 165 (2007) 307–314.
[35] Y. Zhao, J. Chen, J. Power Sources 186 (2009) 96–103.
[36] Z. Yan, J. Chen, J. Appl. Phys. 65 (1989) 1–4.
[37] J. Chen, Z. Yan, J. Chem. Phys. 90 (1989) 4951–4955.
[38] J. Chen, J.A. Schouten, Energy Convers. Manage. 39 (1998) 999–1007.
[39] S.H. Chan, O.L. Ding, Int. J. Hydrogen Energy 30 (2005) 167–179.
[40] D. Sánchez, R. Chacartegui, A. Muñoz, T. Sánchez, J. Power Sources 160 (2006) 1074–1087.
[41] P.G. Bavarsad, Int. J. Hydrogen Energy 32 (2007) 4591–4599.
[42] J. Chen, B. Andresen, Heat Recovery Syst. CHP 15 (1995) 723–731.
[43] D. Sánchez, A. Muñoz, T. Sánchez, J. Power Sources 169 (2007) 25–34.